Available online at www.sciencedirect.com
ScienceDirect
Cement and Concrete Research 37 (2007) 295–302
Cement and Concrete Research

Microstructure and texture of hydrated cement-based materials: A proton field cycling relaxometry approach

J.-P. Korb [a,*], L. Monteilhet [a], P.J. McDonald [b], J. Mitchell [b]

[a] Laboratoire de Physique de la Matière Condensée, UMR 7643 du CNRS, Ecole Polytechnique, 91128 Palaiseau, France
[b] School of Electronics and Physical Sciences, University of Surrey, Guildford, Surrey, GU2 7XH, UK

Received 18 November 2005; accepted 3 August 2006

Abstract

We show how the measurement of proton nuclear magnetic spin-lattice relaxation as a function of magnetic field strength (and hence nuclear Larmor frequency) can provide reliable information on the microstructure (specific surface area and pore size distribution) throughout the progressive hydration of cement-based materials. We present in details the experimental and theoretical characteristic features of the relaxation dispersion to support an interpretation in terms of coupled solid–liquid relaxation at pore interfaces, surface diffusion, and nuclear paramagnetic relaxation. The measurement does not require any drying temperature modification and is sufficiently fast to be applied continuously during the progressive hydration of the material. Coupling this method with the standard proton nuclear spin relaxation and high resolution NMR allows us to follow the development of micro-scale texture within the material.

Keywords: NMR relaxation analysis; Field cycling; Specific surface area; Surface dynamics; Microstructure; Cement; Mortar

1. Introduction

The ability to directly and reliably probe the value of the specific surface area, S_p, of a hydrated cement-based material is fundamental to characterize the highly disordered internal porous microstructure of the material. This is all the more important for hardened cement paste where the value of S_p is directly related to the mechanical performance of cement-based materials such as concrete. However, most of the existing techniques have been shown to be largely inadequate. Widely dispersed values of S_p ranging from 80 to 300 m^2/g have been obtained previously [1], by, for instance: nitrogen gas sorption [2], mercury intrusion [3], small-angle X-rays (SAXS [4]) and neutron scattering (SANS [5]) and nuclear magnetic relaxation (NMR [6–8]). Gas sorption requires a preliminary drying and is limited to accessible pores. Mercury intrusion requires high pressures that perturb the pore structure. NMR measurements for proton [6] and deuteron [7] have used only a single high frequency that makes the separation of the surface and bulk contributions from the overall measured relaxation rate difficult. Moreover, some of these NMR measurements require successive liquid saturation and drying [6] or use of cryoporometry [9] that might perturb the microstructure.

We propose a new NMR approach to probe the surface dynamics of proton species directly and obtain the specific surface area for a hydrated cement-based material that does not require any drying or temperature modification. Our method is based on a clear separation of surface and bulk contributions of the overall ^{1}H nuclear spin-lattice relaxation rate (R_1) of water confined within the hydrated cement. For this purpose, we measure the variation of R_1 as a function of magnetic field strength; the nuclear magnetic relaxation dispersion (NMRD). We have shown in various calibrated microporous media [10,11], rocks [12,13], and mortars [14] that the benefit of exploring the low frequency range is to clearly isolate the typical NMRD dispersion features associated with different processes of molecular surface dynamics. Here we outline our previously proposed model [14] based on solid–liquid cross-relaxation, proton surface diffusion, nuclear paramagnetic relaxation, and high resolution NMR [15] in the presence of progressive hydration to interpret the remarkable features of the proton NMRD in different cement-based materials. This allows us to

* Corresponding author.
E-mail address: jean-pierre.korb@polytechnique.fr (J.-P. Korb).

0008-8846/$ - see front matter © 2006 Elsevier Ltd. All rights reserved.
doi:10.1016/j.cemconres.2006.08.002

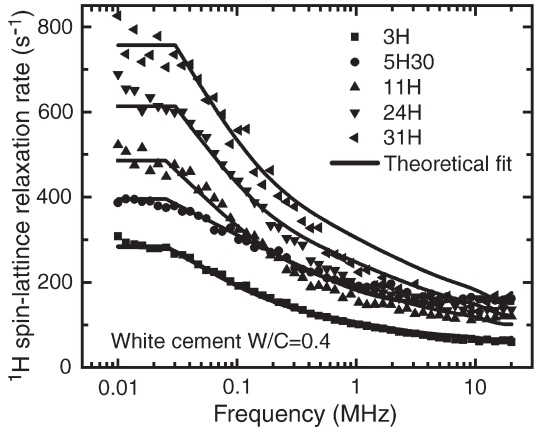

Fig. 1. Measured ^{1}H spin-lattice relaxation rate as a function of the Larmor frequency in white cement (w/c=0.4) for different durations of hydration. The continuous lines are the best fits obtained with Eqs. (2)–(5).

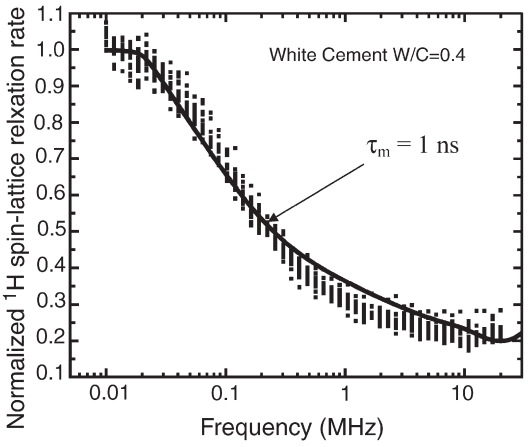

Fig. 2. Renormalization of the data presented in Fig. 1 for all hydration times. The continuous line is the best fit obtained with Eq. (6).

probe directly the dynamics of proton species at the surface of CSH and the specific surface area of these materials.

The determination of the pore size distribution is also very important for characterizing the microstructure of cementitious material. However, exploring the porosity in the micropore range is so far poorly described because most of existing methods are invasive and perturbating. We have recently proposed an original method based on both proton nuclear magnetic relaxation dispersion and high resolution NMR spectra to investigate the microstructure of synthesized Ca_3SiO_5 hydrated cement paste [15]. This method allows a clear assessment of the local proton chemical sites as well as the determination of dynamical information of moving proton species in pores. Here, we just present an application of the proton field cycling relaxometry to evidence the pore size distribution of a 1-year-old C_3S paste between 1.8 and 600 nm. One should also mention some recent 2D correlation relaxometry experiment that proved to be also a particularly sensitive probe of pore-water dynamics providing, in complement to field cycling relaxometry, direct information on pore size distribution and exchange of water between the gel and capillary pore networks [16].

2. Materials

Cement pastes were prepared using Ketton white cement, obtained from Castle Cement. White cement was used because of its low content of paramagnetic constituents. We carefully measured and mixed the amount of cement and distilled water for a water-to-cement (w/c) ratio of 0.4. We put the early paste into a small tube 0.7 cm in diameter and 5 cm long to a depth of 1 cm. The sample was then covered by a small quantity of water to ensure the pore structure remained saturated during the curing time. We closed the small tube with PTFE (Teflon) tape and inserted it into a larger NMR tube, 20 cm long and 1 cm diameter. The mortar sample was prepared by mixing cement, sand, silica fume, water and superplasticizer with a w/c ratio of 0.65; more details on this sample can be found in Ref. [14]. The C_3S sample was synthesized by calcination of stoichiometric mixture of $CaCO_3$ and silica at high temperature (1100 °C) with a variable amount of Fe_2O_3. Ca_3SiO_5 was ground to a mean particle size of 10 μm. The material has been prepared with a very low iron oxide (Fe_2O_3) mass ratio of 0.05% to facilitate the field cycling relaxometry measurements of a 1-year-old material.

3. Results

We present the variation of R_1 as a function of proton Larmor frequency or nuclear magnetic relaxation dispersion (NMRD) of water in hydrated white cement pastes (Figs. 1 and 2), OPC (Fig. 3) and mortar (Figs. 4 and 5) collected for all durations of hydration. The measurements have been performed at 25 °C over a large range of Larmor frequencies from 10 kHz up to 20 MHz using a Fast Field Cycling NMR spectrometer manufactured by *Stelar*. These NMRD data have been renormalized following a method presented below in the theoretical section. We note two remarkable features in the frequency dependence of all these NMRD data.

(i) There is a plateau below a cross-over frequency $\omega_d \sim 22$ kHz that corresponds to the residual proton dipole–dipole energy in the solid state.

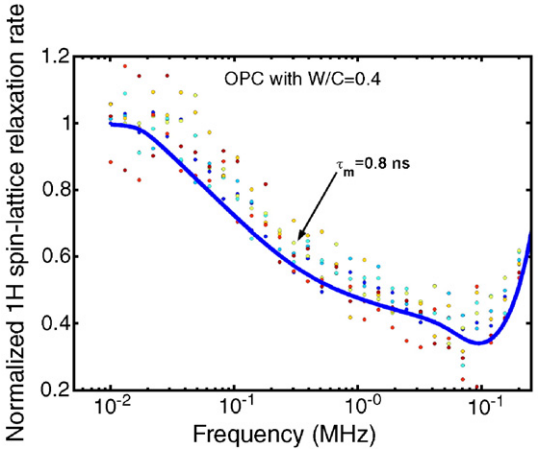

Fig. 3. Renormalization of the measured ^{1}H spin-lattice relaxation rate as a function of the Larmor frequency in OPC (w/c=0.4) for all hydration times. The continuous line is the best fit obtained with Eq. (6).

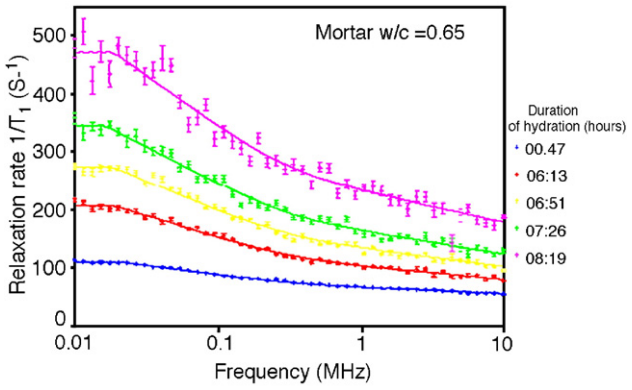

Fig. 4. Measured ^{1}H spin-lattice relaxation rate as a function of the Larmor frequency in mortar (w/c=0.65) for different durations of hydration. The continuous lines are the best fits obtained with Eqs. (2)–(5).

(ii) Above ω_d, one observes a bi-logarithmic dispersion behavior, characterized by a 10/3 slope ratio, for every duration of hydration. This frequency behavior is unambiguously consistent with a two-dimensional proton-water diffusion in the proximity of the paramagnetic relaxation centers [10–14].

The renormalization proves that the same nuclear magnetic relaxation process occurs for any duration of hydration. The unique cross-over frequency ω_d is indicative of a fundamental modification in the relaxation when the correlation time reaches the value $\tau_{rigid} \sim 1/\omega_d = 7.2$ μs which appears to be due to the cross-relaxation between solid and mobile proton species.

The amount of paramagnetic ferric ions was evaluated through a double integration of an Electron Spin Resonance (ESR) spectrum obtained using an ESR Bruker spectrometer operating at 9.6 GHz (Fig. 6). We calculated a quantity of $\eta_S = 1.67 \times 10^{18}$ paramagnetic ions Fe^{3+} per gram of dry material and a negligible amount of Mn^{2+}. The ESR spectrum was calibrated by including a single monocrystal of $CuSO_4$ with a precisely measured mass in our sample. Assuming a uniform density of paramagnetic impurities, we can deduce a population of surface Fe^{3+} impurities as $\sigma_S = \eta_s \rho_d \xi = 2.5 \times 10^{11}$ Fe^{3+}/cm^2, where $\rho_d = 2.5$ g/cm^3 is the density of the material, and $\xi = 6$ Å is the average interlayer distance between two Fe^{3+} impurities [17] to which the relaxation of liquid protons in the saturated porous media is sensitive.

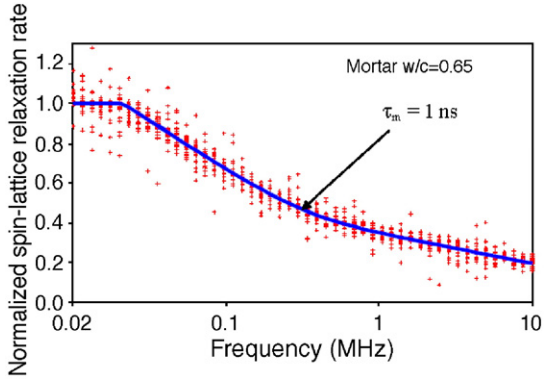

Fig. 5. Renormalization of the data presented in Fig. 4 for all hydration times. The continuous line is the best fit obtained with Eq. (6).

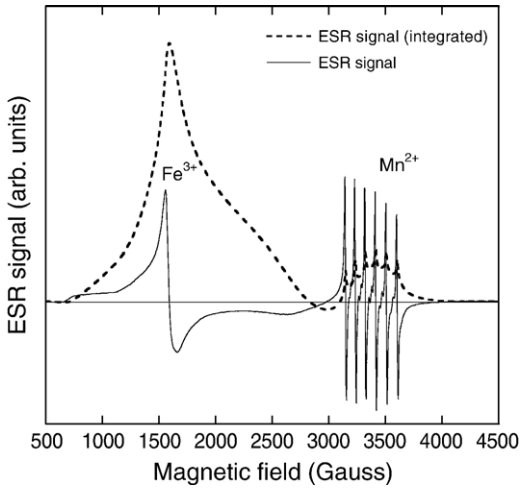

Fig. 6. Electron spin resonance spectra of a dry white cement powder. We display in the same plot the integrated spectrum obtained after correction of the baseline. This clearly shows the importance of the contribution coming from Fe^{3+} ions in comparison to Mn^{2+} ions.

We have followed the progressive hydration of the paste by measuring the ^{1}H spin-lattice relaxation rate at a single Larmor frequency of 10 kHz (Fig. 7). This allowed us to monitor the hydration from a few minutes to several days. Each experiment requires an intrinsic duration ranging from 2 min (at early stage of hydration) to 1 h (in later stages) to maintain an acceptable signal-to-noise ratio. The method has been extended to follow the pore size distribution at very long times for a 1-year-old C_3S-paste sample (Fig. 9). Here the proton relaxation presents a multiexponential longitudinal magnetization decay. But all the dispersion curves associated to each of the individual relaxation rates present the same dispersion curves (NMRD) while they are scaled as the surface to volume ratio of separated pore sizes.

4. Theory of nuclear magnetic relaxation dispersion (NMRD) in cementitious materials

In a previous publication [14] we proposed a theoretical model that reproduces all the relaxation features reported in Figs. 1–5 and 9. Here, we just outline the essential features of such a model. Basically, when considering the nuclear relaxation of water embedded in solid hydrated cement, there are two longitudinal magnetizations associated with the liquid and solid: m_w and m_s, respectively (Fig. 8a). Introducing the dimensionless variable for the departure from equilibrium $M(t) = [m(t) - m^{eq}]/m^{eq}$, these two spin magnetizations are coupled through the cross-relaxation at the solid–liquid interface and are also coupled to the lattice as follows [14]:

$$\frac{d}{dt}\begin{pmatrix} M_s(t) \\ M_w(t) \end{pmatrix} = -\begin{pmatrix} R_{1,s} + k/F & -k/F \\ -k & R_{1,w} + k \end{pmatrix}\begin{pmatrix} M_s(t) \\ M_w(t) \end{pmatrix}. \quad (1)$$

where $R_{1,w}$ and $R_{1,s}$ are the spin-lattice relaxation rates for the confined liquid-proton water and solid protons in the solid hydrates, respectively. k is the dipolar cross-relaxation rate from the water protons to the solid-proton species, and F is the ratio of the solid-proton population to the liquid-proton population at

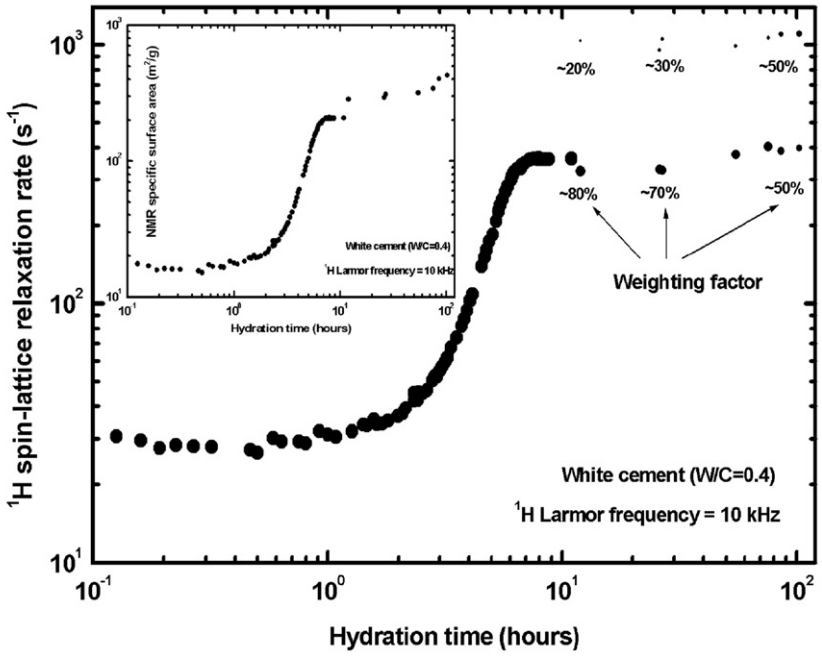

Fig. 7. ^{1}H spin-lattice relaxation rate as a function of the hydration time measured at a Larmor frequency of 10 kHz in white cement (w/c=0.4). We note a bi-exponential relaxation behavior after 10 h of hydration. The weighting factors for each of the relaxation components are indicated. The inset represents the NMR specific surface area deduced from the data in the main figure using Eqs. (2) and (3).

equilibrium: $F=m_s^{eq}/m_w^{eq}$ (Fig. 8a). The solutions of Eq. (1) are bilinear combinations of exponentials with fast (R_{fast}) and slow (R_{slow}) recovery terms given by the eigenvalues of the matrix of Eq. (1). However, with the fast-field cycling spectrometer, one observes only the slow recovery term, R_{slow}:

$$R_{slow}=\frac{1}{2}\left\{R_{1,s}+R_{1,w}+k(1+1/F)-[[R_{1,s}-R_{1,w}-k(1-1/F)]^2+4k^2/F]^{1/2}\right\} \quad (2)$$

We have also recently proposed a theoretical model for the proton Larmor frequency dependence of $R_{1,w}(\omega_I)$ [14]. Basically, we consider a large number of protons (I) in spin-bearing water molecules diffusing in pores with a surface density σ_S of fixed Fe^{3+} paramagnetic impurities (S) (Fig. 8b). Since the gyromagnetic ratio of the electron, γ_S, is much larger than that of the proton, γ_I ($\gamma_S=658.21\gamma_I$), the reduced liquid proton spin-relaxation rate $R_{1,w}$ is due to the modulation of the dipole–dipole interactions between the I and S spins through translational diffusion. The model proposed is built on the following considerations:

(i) The interpretation of the relaxation curves in Figs. 1–5 and 9 is based on the general biphasic fast-exchange model between the protons transiently belonging to the surface and the bulk in a given pore [18]. This model assumes that the molecular exchange between these two phases is faster than individual proton relaxation times. A consequence of this model is a drastic enhancement of the surface contribution of $R_{1,w}$ in Eq. (2), especially at low frequencies and for a microporous media where the surface to volume ratio S/V is very large [10,11].

(ii) The main contribution of the proton relaxation $R_{1,w}$ at low frequencies comes from the two-dimensional diffusion of the water molecules across the pore surface near the fixed relaxing sinks S that modulates the dipole–dipole interaction between the proton species and the Fe^{3+} ions fixed at the surface [10,11,14].

(iii) The numerous two-dimensional I–S molecular reencounters are responsible for the net frequency dependence observed for the longitudinal spin-relaxation rate $R_{1,w}$.

(iv) The residence time of the liquid at the pore surface depends on the existence of potential chemical bonds with specific surface groups.

(v) At high frequencies (10–100 MHz), the electron paramagnetic relaxation controls the proton relaxation [19,20].

Taking these considerations into account, we find that the following theoretical analytical expression of $R_{1,w}$ allows us to reproduce all the observed frequency features after substitution into Eq. (2):

$$R_{1,w}(\omega_I>\omega_d)=R_{1,bulk}+\frac{x\varepsilon}{60}\sigma_S\rho_w S_{p,NMR}(\gamma_I\gamma_S\hbar)^2S(S+1) \times\left\{\frac{\pi}{\varepsilon^4}\tau_m\left[7\ln\left(1+\frac{1}{\omega_S^2\tau_m^2}\right)+3\ln\left(1+\frac{1}{\omega_I^2\tau_m^2}\right)\right] +\frac{8n\varepsilon^2}{r_{IS}^6}\tau_c\left[\frac{7}{1+\omega_S^2\tau_c^2}+\frac{3}{1+\omega_I^2\tau_c^2}\right]\right\} \quad (3)$$

where $\omega_d\sim22$ kHz corresponds to the residual proton dipole–dipole energy in the solid state. ρ_w is the density of the water, $\varepsilon=3.8$ Å is the water molecule size, and $x\varepsilon\sim10$ Å is an interfacial water layer according to previous calorimetry and NMR studies [21]. One has $x\varepsilon\rho_w S_{p,NMR}=N_s/N$ which is the ratio of the number of water molecules at the pore surface,

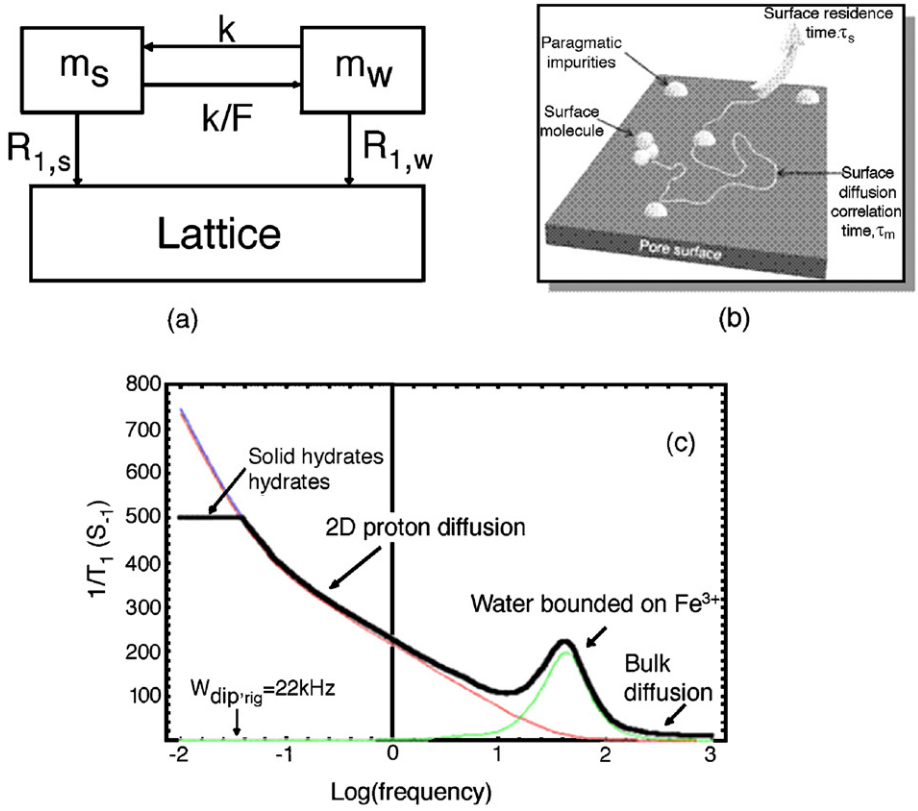

Fig. 8. (a) Schematic diagram of coupled magnetizations between liquid, solid and lattice. The various relaxation rates are indicated. (b) Schematic diagram of the two-dimensional diffusion of water molecules in vicinity of Fe^{3+} ions on the solid–liquid pore surface interface. The correlation time for molecular jumps is τ_m; the surface residence time is τ_s (approximately equal to τ_{rigid}, see text). (c) Calculated frequency dependence of R_{slow} from Eqs. (2)–(5). We have presented the main contributions of Eq. (3) in light continuous lines and the overall result given by Eqs. (2) and (3) as a bold line.

N_s, to the total number, N, of exchangeable water molecules in the sample, and $S_{p,NMR}=S_pF$ is the NMR-based value of the specific surface area S_p. Also in Eq. (3), τ_m is the correlation time characterizing the two-dimensional diffusion of the proton species at the surface of the pores; $r_{IS}=2.7$ Å is the distance of minimal approach between I and S spins, $S=5/2$ for Fe^{3+}; n is the population of bounded water molecules in the ligand field of the Fe^{3+} ions. The correlation time τ_c of the nuclear paramagnetic relaxation is given by $1/\tau_c=1/\tau_{ex}+1/T_{1Fe}\approx 1/T_{1Fe}$ where τ_{ex} ($\tau_{ex}\gg T_{1Fe}$) is the lifetime of water in the ligand field of the ferric ions. The electronic spin-lattice relaxation time of the paramagnetic impurity T_{1Fe} (of the order of 10^{-11} s) is defined as $T_{1Fe}^{-1}(\omega_S)=H_S^2\tau_v\left[(1+\omega_S^2\tau_v^2)^{-1}+4(1+4\omega_S^2\tau_v^2)^{-1}\right]$ [19,20], where τ_v is the correlation time for the electron-lattice relaxation interaction and H_S^2 is the intensity of the electronic spin fluctuations. The relaxation rate in the bulk phase, $R_{1,bulk}\sim 0.5\ s^{-1}$ is caused by the fast molecular reorientations and translations and is independent of frequency in the low field range studied [22].

Substituting Eq. (3) into Eq. (2) gives the calculation of the frequency dependence of $R_{slow}(\omega_I)$ displayed in Fig. 8c. We have plotted individually (in light continuous lines) the main effects of the different components of Eq. (3). The overall frequency dependence is shown by the bold line.

When $\omega_I<\omega_d=22$ kHz, and $k\ll R_{1,w}$, $R_{1,s}$, and $(R_{1,w}-R_{1,s})$, $F\ll 1$, the system reaches a long correlation time limit typical of the rigid-lattice limit: $\tau_{rigid}=1/\omega_d=7.2$ μs. The cross-relaxation becomes very efficient ($k/F\gg k$) and is only limited by the transfer of dipolar energy (spin diffusion). Under these conditions Eq. (2) simplifies to:

$$R_{slow}(\omega_I<\omega_d)\approx R_{1,s}+k/F,\ \text{with } R_{1,s}\equiv R_{1,w}(\omega_I=\omega_d) \qquad (4)$$

The observed plateau below ω_d is thus characteristic of the rigid-lattice limit of the solid-proton hydrates. The absolute value of such a plateau is thus indicative of the specific area precisely at the solid–liquid interface. This plateau has thus been useful to follow directly the time evolution of the specific surface area (Fig. 7).

When $\omega_I>\omega_d$ and for $k\ll R_{1,w}$, $R_{1,s}$ and $(R_{1,s}-R_{1,w})$, $F\ll 1$, the system experiences correlation times typical of a surface liquid with correlation times much shorter than τ_{rigid}. Here Eq. (2) simplifies to:

$$R_{slow}(\omega_I>\omega_d)\approx R_{1,w}(\omega_I>\omega_d)+k \qquad (5)$$

i.e. the relaxation is dominated by the surface water-proton dynamics as shown by the typical bi-logarithmic dispersion curves displayed in Fig. 8c.

When 10 MHz $\le\omega_I\le$ 100 MHz, the nuclear paramagnetic relaxation is dominant and enhances the relaxation in a narrow band in the highest frequency range of our measurements. Its contribution appears when a certain population of bounded

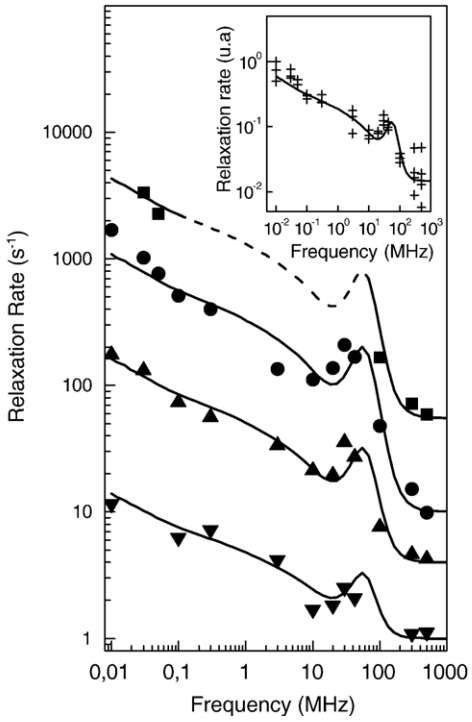

Fig. 9. Logarithmic plot of the dispersion curves showing the four longitudinal relaxation rates $1/T_1$ versus the external magnetic field expressed in terms of the Larmor frequencies of the proton for a C_3S paste hydrated 1 year with w/c=0.4 at room temperature. The four curves have been successfully renormalized in the inset. The continuous lines correspond to the best fit obtained by the relaxation model using Eq. (3).

water molecules (typical value of $n \sim 2$) exists in the ligand field of the Fe^{3+} ions. We see in the high frequency part of Fig. 3, the beginning of such an enhancement. We show in Fig. 9 some characteristic frequency dependence (a bump around 60 MHz), realized on aged C_3S pastes, that are typical of this relaxation process.

When $\omega_I > 100$ MHz, one reaches the usual domain of fast bulk dynamics where the relaxation becomes almost frequency independent.

5. Discussion of nuclear magnetic relaxation dispersion (NMRD) in cementitious materials

5.1. Surface diffusion coefficient

The limiting expressions (Eqs. (4) and (5)) indicate the way to renormalize the collected NMRD data $R_{slow}(\omega_I, t)$ obtained for all durations, t, of hydration and provides the correlation time (mean jump time τ_m) for water diffusing on pore surfaces. By subtracting the limiting constant bulk value $R_{1,bulk}$ at high frequencies and dividing the resulting data by the value of the respective low frequency plateau, one has:

$$R_{slow}^{norm}(\omega_I, t) = \frac{R_{slow}(\omega_I, t) - R_{1,bulk}}{R_{slow}(\omega_I < \omega_d) - R_{1,bulk}} = \frac{R_{slow}(\omega_I, t) - R_{1,bulk}}{R_{1,w}(\omega_I = \omega_d) + k/F - R_{1,bulk}} \quad (6)$$

As almost all the parameters present in Eqs. (2)–(6) are either known or measured independently, we can fit easily the NMRD data presented as continuous lines in Figs. 1–5 and 9. First we use Eq. (6) to obtain the surface translational correlation time τ_m from a single parameter fit of (Figs. 2, 3 and 5). We find similar results for various cement-based materials: white cement paste (Figs. 1 and 2), OPC (Fig. 3) and mortar (Figs. 4 and 5), which suggests a quasi-universality and pore scale invariance of the water dynamics on the pore surface in CSH with τ_m approximately equal to 1 ns. Finally, one deduces the translational diffusion coefficient D_{surf} at the pore surface from Stokes–Einstein relation: $D_{surf} = \varepsilon^2/(4\tau_m)$ that is about 1/60 of that of bulk water (Table 1). These values of the diffusion coefficients of water in hydrated cement pastes and mortars obtained from proton field cycling NMR spin-lattice relaxation over three orders of magnitude in magnetic field strength are in good agreement with values from molecular dynamics simulations of water on the surface of tobermorite [23]. The level of agreement from these two independent approaches provides support for their validity.

5.2. Specific surface area

Concerning the measurement of the NMR specific surface area $S_{p,NMR}$, we have enlarged the potential use of proton field cycling up to 100-h-old white cement paste by measuring the time evolution of the spin-lattice relaxation rate $R_{1,w,observed}(\omega_I = 10$ kHz, $t)$ only at a single very low frequency (10 kHz). At 10 kHz, we have shown that one probes only the relaxation rate coming from the solid hydrates ([14,15]). Moreover at this low frequency, one can neglect the bulk and the nuclear paramagnetic contributions in Eq. (3) (see Fig. 8c). One can thus obtain the following expression of

Table 1
Results on surface diffusion of proton species for different cement-based materials

Samples	OPC, w/c=0.4	OPC+10% PVA (latex)	Ketton white cement+ excess of water	Ketton white cement, w/c=0.4	Mortar+silica fume+ adjuvant
Correlation time of translational diffusion at the pore surface	0.8 ns	0.07 ns	1.2 ns	1 ns	1 ns
Translational diffusion coefficient at the pore surface D_{surf}	4.5×10^{-7} cm^2/s	5.2×10^{-6} cm^2/s	3.0×10^{-7} cm^2/s	3.6×10^{-7} cm^2/s	3.6×10^{-7} cm^2/s
D_{surf}/D_{bulk}	1/49	1/4.2	1/73	1/61	1/61

the NMR specific surface area $S_{p,NMR}$ that is directly proportional to $R_{1,w,observed}(\omega_I = 10\ kHz,\ t)$:

$$S_{p,NMR}(t) = \frac{R_{1,w,observed}(\omega_{I,10\ kHz}, t)}{\left\{\frac{\chi_E}{60}\sigma_s\rho_w(\gamma_I\gamma_S\hbar)^2 S(S+1)\frac{\pi}{5}\tau_m\left[7\ln\left(1+\frac{1}{659^2\omega^2_{I,10\ kHz}\tau^2_m}\right)+3\ln\left(1+\frac{1}{\omega^2_{I,10\ kHz}\tau^2_m}\right)\right]\right\}} \quad (7)$$

where all the terms in the denominator of the rhs of Eq. (7) is known or measured. We present in Fig. 7 the variation of $R_{1,w,observed}(\omega_I = 10\ kHz,\ t)$ with the hydration time in white cement paste (w/c = 0.4). An interesting feature is the bi-exponential character of the relaxation observed after 10 h of hydration. Here one notes two branches in the time evolution of $R_{1,w,observed}(\omega_I = 10\ kHz,\ t)$ whose relative intensity changes with time. The inset of Fig. 7 shows the time evolution of the NMR specific surface area, $S_{p,NMR}$, obtained from this experiment with Eqs. (2) and (3) and the value found for τ_m. It is interesting to note that, after the setting period, $S_{p,NMR}$ continues to slightly increase with hydration similarly with the evolution of the degree of chemical advancement measured from calorimetry.

5.3. Pore size distribution

Fig. 9 shows the NMRD curves of a 1-year-old C_3S sample. The renormalization of all these dispersion curves to a single one, shown in the inset of Fig. 9, proves that the same relaxation process occur at each of the four classes of relaxation rates from 1 to 4000 s^{-1}. The continuous lines in Fig. 9 are the best fits obtained with Eq. (3). At low frequencies, as shown in the theoretical section, the relaxation is due to the modulation of dipole–dipole interaction between the two-dimensional diffusing proton species and the Fe^{3+} ions fixed at the surface [14]. At high frequencies, the electron paramagnetic relaxation controls the proton relaxation [19,20]. This mechanism leads to a characteristic peak observed in the 10–100 MHz. The frequency dependence of the overall spin-lattice relaxation rate, mainly due to the surface contribution, shows that the renormalization factors for the four classes of the relaxation rates are proportional to the surface to volume ratio. Provided that the amount of paramagnetic ferric ions is evaluated through a calibrated electronic spin resonance (ESR) experiment (Fig. 6), these renormalization factors lead to the following values of average pore sizes $\langle R_i \rangle = \{1.8, 7.0, 50 \text{ and } 600\ nm\}$. Such a discrete pore size distribution obtained at long times in a range of length scales between 2 and 600 nm is typical to previous nuclear relaxation works on cement pastes that observed several distinct relaxation rates that were attributed to the existence of different pore sizes [24–31]. It is also supported by recent cryoporometry of Valckenborg et al. [30]. The most plausible interpretation is that the first two smaller pore sizes are associated with the interbrick and intercrystallites of CSH comprising the gel, while the last two larger sized pores are associated to packing defects and capillary pores. We have studied in detail in Ref [15] how these pore sizes evolve in time and reach progressively a hierarchical surface fractal distribution. Some of these results are confirmed by recent 2D correlation spin relaxation study [16].

6. Conclusion

Based on proton magnetic relaxation dispersion (NMRD) of various cement-based materials, we have proposed a continuous and direct measurement of surface dynamics of proton species τ_m and specific surface area $S_{p,NMR}$ of various cement-based materials. This technique allows a clear separation of the NMRD of mobile water at the surface of the pores from that of the bulk. Though $S_{p,NMR}$ ranges within the results of most other techniques, there are several advantages in favour of our measurements. (i) Proton NMRD is neither invasive nor destructive because one measures the response of the mixing water itself in the normal saturated state of cement. No liquid or gas intrusion, no drying or other temperature and pressure modifications are required that risk damaging the microstructure. (ii) The measurement is sufficiently fast to be applied continuously during the progressive hydration and setting of the material. (iii) The remarkable features of the proton NMRD at low frequency allow one to probe directly the proton surface dynamics that contribute to $S_{p,NMR}$. The technique has also been applied to characterize the average pore sizes and distribution.

Acknowledgements

We thank the NANOCEM Consortium for financial support. JM thanks The Royal Society for financial support. JPK thanks Dr. C. Chachaty for help in the ESR analysis, F. Barberon for the NMRD results of mortars, and ATILH and LAFARGE for financial support.**[KS]**

References

[1] J.J. Thomas, H.M. Jennings, A.J. Allen, The surface area of hardened cement paste as measured by various techniques, Concr. Sci. Eng. 1 (1999) 45–64.
[2] R.L. Rarick, J.I. Bhatty, H.M. Jennings, Surface area measurement using gas sorption: application to cement paste, Material Science of Concrete, vol. IV, ACS, Westerville, OH, 1994, pp. 1–36.
[3] E. Sauzeat, Thesis, Institut National Polytechnique de Lorraine, Nancy 1998.
[4] D.N. Winslow, S. Diamond, Specific surface of hardened cement paste as determined by small-angle X-ray scattering, J. Am. Chem. Soc. 57 (1974) 193–197.
[5] A.J. Allen, Time-resolved phenomena in cements, clays and porous rocks, J. Appl. Crystallogr. 24 (1991) 624–634.
[6] W.P. Halperin, F. d'Orazio, F. Bhattacharja, J.C. Tarczon, Magnetic resonance relaxation analysis of porous media, in: J. Klafter, J.M. Drake (Eds.), Molecular Dynamics in Restricted Geometries, J. Wiley, NY, 1989, pp. 311–350.
[7] R. Maggion, Thesis, Université d'Orléans (1992).
[8] L. Barbic, I. Kocuvan, R. Blinc, G. Lahajnar, P. Merljak, I. Zupancic, The determination of surface development in cement pastes by nuclear magnetic resonance, J. Am. Ceram. Soc. 65 (1982) 25–31.
[9] R.M.E. Valckenborg, L. Pel, K. Kopinga, Combined NMR cryoporometry and relaxometry, J. Phys. D: Appl. Phys. 35 (2002) 249–256.
[10] J.-P. Korb, M. Whaley, R.G. Bryant, Translational diffusion of liquids at surfaces of microporous materials: a field cycling magnetic relaxation study, Phys. Rev., E 56 (1997) 1934–1945.
[11] J.-P. Korb, M. Whaley-Hodges, Th. Gobron, R.G. Bryant, Anomalous surface dynamics of water and aprotic liquids in nanopores, Phys. Rev., E 60 (1999) 3097.
[12] S. Godefroy, J.-P. Korb, M. Fleury, R.G. Bryant, Surface nuclear magnetic relaxation and dynamics of water and oil in macroporous media, Phys. Rev., E 64 (2001) 021605.

[13] S. Godefroy, M. Fleury, F. Deflandre, J.-P. Korb, Temperature effect on NMR surface relaxation in rocks for well logging applications, J. Phys. Chem. 106 (2002) 11183.
[14] F. Barberon, J.-P. Korb, D. Petit, V. Morin, E. Bermejo, Probing the surface area of a cement-based material by nuclear magnetic relaxation dispersion, Phys. Rev. Lett. 90 (2003) 116103–116104.
[15] A. Plassais, M.-P. Pomies, N. Lequeux, J.-P. Korb, D. Petit, F. Barberon, Microstructure evolution of hydrated cement pastes, Phys. Rev., E 72 (2005) 041401.
[16] P.J. McDonald, J.-P. Korb, J. Mitchell, L. Monteilhet, Surface relaxation and chemical exchange in hydrating cement pastes: A two-dimensional NMR relaxation study, Phys. Rev., E 72 (2005) 011409.
[17] P. Faucon, thesis, University de Cergy Pontoise, France.
[18] K.R. Brownstein, C.E. Tarr, Phys. Rev., A 19 (1979) 2446.
[19] I. Solomon, Relaxation processes in a system of 2 spins, Phys. Rev. 99 (1955) 559–565.
[20] N. Bloembergen, L.O. Morgan, Proton relaxation times in paramagnetic solutions effects of electron spin relaxation, J. Chem. Phys. 34 (1961) 842–848.
[21] J.J. Fripiat, M. Letellier, P. Levitz, Philos. Trans. R. Soc. Lond., A 311 (1984) 287.
[22] A. Abragam, The Principles of Nuclear Magnetism, Clarendon, Oxford, 1961 Ch 8.
[23] J.-P. Korb, P.J. McDonald, L. Monteilhet, A.G. Kalinichev, R.J. Kirkpatrick, Comparison of proton field-cycling relaxometry and molecular dynamics simulations for proton-water surface dynamics in cement-based materials, Cement and Conc. Res. (in press).
[24] R. Blinc, G. Lahajnar, S. Zumer, M.M. Pintar, Phys. Rev., B 38 (1988) 2873.
[25] W.P. Halperin, J.Y. Jehng, Y.Q. Song, Magn. Reson. Imaging 12 (1994) 169.
[26] J.Y. Jehng, D.T. Sprague, W.P. Halperin, Magn. Reson. Imaging 14 (1996) 785.
[27] A.J. Bohris, U. Goerke, P.J. McDonald, M. Mulheron, B. Newling, B. Le Page, Magn. Reson. Imaging 16 (1998) 455.
[28] S. Philippot, J.-P. Korb, D. Petit, H. Zanni, Magn. Reson. Imaging 16 (1998) 515.
[29] R.M.E. Valckenborg, L. Pel, K. Hazrati, K. Kopinga, J. Marchand, Mat. Struct. 34 (2001) 599.
[30] R.M.E. Valckenborg, L. Pel, K. Kopinga, Combined NMR cryoporometry and relaxometry, J. Phys., D, Appl. Phys. 35 (3) (2002) 249.
[31] C. Porteneuve, J.P. Korb, D. Petit, H. Zanni, Cem. Concr. Res. 32 (2002) 97.